

Engineering Entangled Coherent States of Magnons and Phonons via a Transmon Qubit

Marios Kounalakis,^{1,2,*} Silvia Viola Kusminskiy,² and Yaroslav M. Blanter¹

¹*Kavli Institute of Nanoscience, Delft University of Technology, 2628 CJ Delft, The Netherlands*

²*Institute for Theoretical Solid State Physics, RWTH Aachen University, 52074 Aachen, Germany*

(Dated: September 29, 2023)

We propose a scheme for generating and controlling entangled coherent states (ECS) of magnons, i.e. the quanta of the collective spin excitations in magnetic systems, or phonons in mechanical resonators. The proposed hybrid circuit architecture comprises a superconducting transmon qubit coupled to a pair of magnonic Yttrium Iron Garnet (YIG) spherical resonators or mechanical beam resonators via flux-mediated interactions. Specifically, the coupling results from the magnetic/mechanical quantum fluctuations modulating the qubit inductor, formed by a superconducting quantum interference device (SQUID). We show that the resulting radiation-pressure interaction of the qubit with each mode, can be employed to generate maximally-entangled states of magnons or phonons. In addition, we numerically demonstrate a protocol for the preparation of magnonic and mechanical Bell states with high fidelity including realistic dissipation mechanisms. Furthermore, we have devised a scheme for reading out the prepared states using standard qubit control and resonator field displacements. Our work demonstrates an alternative platform for quantum information using ECS in hybrid magnonic and mechanical quantum networks.

I. INTRODUCTION

The development of quantum technologies aims towards disruptive practical applications in several fields such as computing, communication and sensing by exploiting the effects of quantum mechanics [1, 2]. The success of this venture largely relies on the evolution of hybrid quantum systems that incorporate the advantages of different physical platforms in a constructive way [3, 4]. For example, circuit quantum electrodynamics (QED), where light-matter interactions in superconducting circuits are used to manipulate quantum information, is one of the leading platforms in quantum computing, combining strong nonlinearities with advanced quantum control and readout as well as high coherence times relative to qubit operations [5, 6]. However, superconducting circuits do not directly couple to optical photons, hindering their integration with optical networks [3]. In this direction, the development of hybrid circuit QED platforms based on mechanical and magnetic systems is an essential requirement towards networked quantum computation [4]. In addition, the evolution of high-quality mechanical systems operating in the quantum regime provides unique opportunities not only in transduction but also in building quantum memories and sensors [3, 4, 7]. Moreover, hybrid quantum systems based on magnons, i.e., the quanta of the collective spin excitations in magnetic materials, offer distinctive advantages, such as unidirectional propagation and chiral coupling to phonons and photons [8, 9], making them prime candidates for technological applications in quantum information sciences [10, 11].

The ability to generate entanglement is at the heart of most protocols in quantum information. For macroscopic mechanical and magnonic resonators, which carry bosonic degrees of freedom and typically operate in the

linear regime, the special class of entangled coherent states (ECS) [12, 13] is of particular interest. Such states exhibit continuous-variable entanglement between different bosonic modes and provide a valuable resource for quantum teleportation [14, 15], quantum computation [16–18] and communication [19, 20]. In addition, ECS are useful for fundamental studies of quantum mechanics with applications in quantum metrology [21, 22] and tests of collapse models [23, 24].

Macroscopic entanglement between mechanical modes has recently been achieved on aluminum drum resonators [25, 26] and micromechanical photonic/phononic crystal cavities [27, 28], however, an experimental demonstration of entanglement between metallic nanobeams such as the ones studied in Refs. [29–31] is currently lacking. Furthermore, while entanglement between atomic ensembles has been experimentally realised in an optical setup [32], entangling magnons in two distant magnets still remains a challenge. Recent theoretical proposals have investigated the possibility of entangling magnons in two Yttrium Iron Garnet (YIG) spheres interacting via photons in a microwave cavity. More specifically, in Ref. [33] the emerging Kerr nonlinearity in strongly driven magnons is used, relying on driving the magnon modes far from equilibrium in order to create entanglement. In Ref. [34] the nonlinearity stemming from the parametric magnetostrictive interaction is employed to create magnon-magnon entanglement, although requiring a much larger magnetostrictive coupling strength than experimentally attainable [35]. Alternatively, in Refs. [36, 37] it is shown that two YIG spheres can be entangled by driving the magnon-cavity system with strong squeezing fields. However, while the above schemes show promise for creating magnon-magnon entanglement in distant YIG spheres, the absence of a highly controllable nonlinear element, such as a qubit, hinders the generation and control of more complex states and ECS, in

particular.

Here we propose a scheme for generating ECS of magnons/phonons in a hybrid circuit QED architecture comprising a superconducting transmon qubit and two magnonic/mechanical modes. Concerning magnonic systems, without loss of generality, we consider two YIG sphere modes in a hybrid qubit-magnon setup similar to Ref. [38], where the qubit-magnon coupling is mediated via a superconducting quantum interference device (SQUID). We showcase a protocol for generating maximally-entangled states such as *Bell* and *NOON* states with high fidelity, by exploiting the parametric nature of the qubit-magnon radiation-pressure interaction and the transmon quantum control toolbox. Furthermore, we analyze a readout scheme for verifying the entanglement in the system based on qubit measurements and displacements of the magnon field. Contrary to previous proposals for generating magnon-magnon entanglement, there is no need for placing the YIG spheres inside a cavity, therefore, increasing scalability and modularity. Furthermore, we numerically demonstrate the validity of our proposal for entangling SQUID-embedded mechanical beam resonators [29–31, 39, 40], thereby extending the possibilities for quantum control using mechanical ECS.

II. HYBRID SYSTEM DESCRIPTION

The fundamental element in the proposed circuit architecture is a dc SQUID, i.e., a superconducting loop interrupted by two Josephson junctions, as schematically depicted in Fig. 1. When shunted by a capacitance C , with charging energy $E_C = 2e^2/C$, this nonlinear inductor can realize a flux-tunable transmon qubit described by the Hamiltonian,

$$\hat{H}_T = 4E_C \hat{N}^2 - E_J \cos \hat{\delta}, \quad (1)$$

where \hat{N} , $\hat{\delta}$ are conjugate operators describing the tunneling Cooper-pairs and the superconducting phase across the SQUID, respectively [41, 42]. In the case where the two junctions are the same (symmetric SQUID), an external flux bias Φ_b tunes the Josephson energy $E_J = E_J^{\max} |\cos \phi_b|$, where $\phi_b \doteq \pi \Phi_b / \Phi_0$ and Φ_0 is the flux quantum.

For magnetic systems, without loss of generality we focus our description on micro-sized YIG spheres similar to Refs. [38, 43]. Upon application of an in-plane magnetic field B_z , a YIG sphere acquires a magnetization M_s and its excitations can be approximated as a set of independent quantum harmonic oscillators with Hamiltonian $\hat{H}_M = \hbar \sum_m \omega_m \hat{a}_m^\dagger \hat{a}_m$, where $a_m^{(\dagger)}$ are bosonic operators describing the annihilation (creation) of single magnons [44, 45]. Note that this description is valid in the limit $\langle \hat{n}^\dagger \hat{n} \rangle \ll N_S$, where N_S is the total number of spins in the sphere [44, 45]. The fundamental excitation, or *Kittel* mode, is a uni-

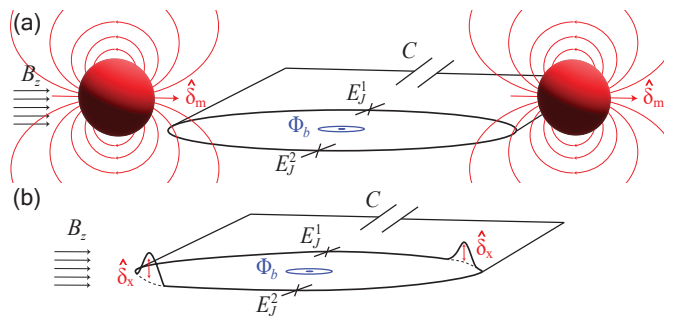


FIG. 1. Proposed hybrid circuit architecture. A flux-tunable transmon qubit, formed by a C-shunted SQUID loop, is coupled to (a) two nearby YIG spheres or (b) two SQUID-embedded mechanical beams. The magnetization of both spheres in (a) is oriented by an in-plane field B_z . The magnetic quantum fluctuations $\hat{\delta}_m$ modulate the SQUID flux as well as the transmon inductive energy, thereby giving rise to a qubit-magnon coupling. In (b) the coupling stems from the mechanical quantum fluctuations $\hat{\delta}_x$ inducing a modulating flux in the SQUID in the presence of the in-plane field B_z . An additional flux bias Φ_b can be externally applied to tune the qubit frequency and modulate the coupling.

formly polarized state of all the spins acting as a single “macrospin” precessing around z , with ferromagnetic resonance (FMR) frequency $\omega_0 = \gamma_0(B_z + B_{\text{ani}})$, where B_{ani} is the anisotropy field [46]. Higher mode frequencies are given by $\omega_m = \omega_0 + \gamma_0 M_s \frac{l-1}{3(2l+1)}$ depending on the magnon angular momentum quantum number l [47].

The mechanical systems of interest in this work consist of SQUID-embedded aluminum beams [29, 30, 39, 48]. Such mechanical beams are realised by suspending part of the SQUID loop such that it can freely oscillate out of plane [29, 30]. Similar to the YIG sphere, its excitations can also be described by a set of independent quantum harmonic oscillators, with Hamiltonian $\hat{H}_X = \hbar \sum_x \omega_x \hat{a}_x^\dagger \hat{a}_x$, where $a_x^{(\dagger)}$ are bosonic operators that annihilate (create) a phonon. The fundamental mode, which is the one considered in this work, oscillates with frequency $\omega_0 = \hbar/(2m x_{\text{zpf}}^2)$, where m is the beam mass and x_{zpf} the magnitude of its zero-point motion [29].

Upon application of an in-plane magnetic field B_z , the quantum fluctuations in the out-of-plane displacement of the beam $\hat{\delta}_x = x_{\text{zpf}}(\hat{a}_x + \hat{a}_x^\dagger)$ induce a flux $\Phi(\hat{\delta}_x) = \beta_0 B_z l \hat{\delta}_x$ through the loop, where l is the beam length and β_0 is a geometric factor that depends on the mode shape [29]. Similarly, quantum fluctuations of the magnetic moment in the magnetized YIG sphere, $\hat{\delta}_m = \mu_{\text{zpf}}(\hat{a}_m + \hat{a}_m^\dagger)$, result in an additional flux $\Phi(\hat{\delta}_m)$ through the SQUID loop. Let us assume that the sphere is placed at an in-plane and out-of-plane distance d from the closest point in the loop. Then in the far-field limit $\Phi(\hat{\delta}_m) = \mu_0 \hat{\delta}_m / (4\sqrt{2}\pi d)$ [38].

The additional flux from each source of quantum fluc-

tuation, $\Phi(\hat{\delta}_j)$, modulates the SQUID flux and consequently its Josephson energy,

$$E'_J(\phi_b, \hat{\delta}_j) \simeq E_J \left(1 - \tan \phi_b \sum_j \phi(\hat{\delta}_j) \right), \quad (2)$$

where we assume $\phi(\hat{\delta}_j) \doteq \pi \Phi(\hat{\delta}_j) / \Phi_0 \ll 1$ and a symmetric SQUID; for a full treatment including finite junction asymmetry see Refs. [38, 39]. Replacing E_J with E'_J in Eq. (1) and expressing the transmon operators in terms of annihilation (creation) operators $\hat{c}^{(\dagger)}$, i.e., $\hat{N} = i[E_J/(32E_C)]^{1/4}(\hat{c}^\dagger - \hat{c})$, $\hat{\delta} = [2E_C/E_J]^{1/4}(\hat{c} + \hat{c}^\dagger)$ [42], yields the total system Hamiltonian

$$\hat{H} = \hat{H}_q + \hbar \sum_j \left[\omega_j \hat{a}_j^\dagger \hat{a}_j - g_j \hat{c}^\dagger \hat{c} (\hat{a}_j + \hat{a}_j^\dagger) \right], \quad (3)$$

where $\hat{H}_q = \hbar \omega_q \hat{c}^\dagger \hat{c} - \frac{E_C}{2} \hat{c}^\dagger \hat{c} \hat{c} \hat{c}$, is the bare transmon Hamiltonian (valid for $E_J \gg E_C$), with qubit frequency $\omega_q = (\sqrt{8E_J E_C} - E_C) / \hbar$ [41].

The last term in Eq. (3) describes the radiation-pressure interaction between the qubit and each bosonic mode, with coupling strength

$$g_j = \frac{\partial \omega_q}{\partial \phi_j} \phi_j^{\text{zpf}}, \quad (4)$$

where ϕ_j^{zpf} is the magnitude of the flux fluctuations induced by either the beam or the magnet, given by $\phi_x^{\text{zpf}} = \pi \beta_0 B_z l x_{\text{zpf}} / \Phi_0$ and $\phi_m^{\text{zpf}} = \mu_0 \mu_{\text{zpf}} / (4\sqrt{2}d\Phi_0)$, respectively. In the case of a symmetric SQUID, the transmon frequency sensitivity to flux changes is

$$\frac{\partial \omega_q}{\partial \phi_j} = \frac{\omega_p}{2} \frac{\sin \phi_b}{\sqrt{\cos \phi_b}}, \quad (5)$$

where $\omega_p = \sqrt{8E_J^{\text{max}} E_C} / \hbar$ is the Josephson plasma frequency at $\phi_b = 2\pi k$ ($k \in \mathbb{Z}$). The behavior of the coupling strength as a function of the SQUID asymmetry and ϕ_b is studied in detail in Ref. [38].

III. ENTANGLED COHERENT STATE GENERATION

The system Hamiltonian in Eq. (3) describes a qubit interacting with a set of bosonic modes via bipartite radiation-pressure interactions. However, in the absence of additional driving, these radiation-pressure couplings lead to interesting dynamics only in the *ultrastrong* coupling regime, $g_j \gtrsim \omega_j$ [39, 49, 50]. Typically, mechanical beam resonators have frequencies of a few MHz [29, 30] and operating magnon frequencies lie above 100 MHz [44, 45], whereas $g_j \lesssim 10$ MHz [38, 39]. Therefore, while the ultrastrong coupling condition seems promising for optomechanical setups [39], it is far from

realistic for magnonic devices. On the other hand, when external driving is introduced to the system, the radiation-pressure interaction can be “activated” even for $g_j < \omega_j$, e.g., by a stroboscopic application of short π qubit pulses [51] or by modulating the coupling [38, 52].

Here, without loss of generality, we consider the case $g_j \ll \omega_j$ and assume that the radiation-pressure interaction is activated by applying a weak flux modulation through the SQUID loop as in Ref. [38]. In this scheme the qubit operates around the transmon “sweetspot”, i.e., $\phi_b \simeq 0$, and an applied ac flux with amplitude ϕ_{ac} at frequency ω_{ac} , modulates the flux, $\phi_b = \phi_{\text{ac}} \cos(\omega_{\text{ac}} t - \theta) \ll 1$, resulting in a modulated coupling strength $g_j(t) = \frac{\omega_p}{2} \phi_j^{\text{zpf}} \cos(\omega_{\text{ac}} t - \theta)$, where θ is a constant phase. In the frame rotating at ω_{ac} the transformed Hamiltonian reads,

$$\hat{\tilde{H}} = \hat{H}_q + \hbar \sum_j \left[\Delta_j \hat{a}_j^\dagger \hat{a}_j - \tilde{g}_j \hat{c}^\dagger \hat{c} (\hat{a}_j e^{i\theta} + \hat{a}_j^\dagger e^{-i\theta}) \right], \quad (6)$$

where $\tilde{g}_j = \frac{\omega_p}{4} \phi_j^{\text{zpf}}$, $\Delta_j = \omega_j - \omega_{\text{ac}}$ and we have omitted fast-rotating terms $\hat{c}^\dagger \hat{c} \hat{a}_j^{(\dagger)} e^{\pm i(\omega_j + \omega_{\text{ac}})t}$ which do not contribute to the dynamics since $\tilde{g}_i \ll (\omega_j + \omega_{\text{ac}})$.

We now describe a simple protocol for generating ECS that are maximally entangled using the Hamiltonian in Eq. (6). Let us assume there are N bosonic modes, interacting with the qubit via bipartite radiation-pressure couplings. First, a microwave pulse, prepares the qubit in a superposition state $|\chi\rangle_q \doteq (|0_q\rangle + e^{i\chi} |1_q\rangle) / \sqrt{2}$. The next step is to activate the bipartite interaction of the qubit with each mode. In the simple case where all the modes we want to entangle have the same frequency, ω_j , then by turning on the flux modulation, i.e., setting $\omega_{\text{ac}} = \omega_j$, for a variable duration, τ_j , the system evolves into a hybrid generalized Greenberger–Horne–Zeilinger state

$$|\psi\rangle_{\text{GHZ}} = \frac{1}{\mathcal{N}} (|0_q 0_1 \cdots 0_N\rangle + e^{i\chi} |1_q \alpha_1 \cdots \alpha_N\rangle), \quad (7)$$

where $|\alpha_j\rangle$ denotes a coherent state with complex phase space amplitude $\alpha_j = -i\tilde{g}_j \tau_j$. For $|\alpha_j| \gtrsim 4$ the normalization factor is $\mathcal{N} \simeq \sqrt{2}$ [53]. Note that if there are M modes with different frequencies, then the flux modulation should be activated M times in order to prepare the state in Eq. (7).

Applying a qubit pulse $R_{\hat{y}, \frac{\pi}{2}}$ followed by a strong projective measurement collapses the qubit in its ground or excited state and projects the bosonic system into $\frac{1}{\mathcal{N}_\pm} (|0_1 0_2 \cdots 0_N\rangle \pm e^{i\chi} |\alpha_1 \alpha_2 \cdots \alpha_N\rangle)$, where the “+” or “−” state results from measuring the qubit in $|0_q\rangle$ or $|1_q\rangle$, respectively. For the case of two bosonic modes with $\tilde{g}_{1,2}, \tau_{1,2}$ chosen such that $\alpha_1 = \alpha_2 = \alpha$ and $\chi = 0$ the prepared state corresponds to the maximally-entangled *Bell* state,

$$|\pm \Psi_{\text{Bell}}\rangle = \frac{1}{\mathcal{N}_\pm} (|00\rangle \pm |\alpha\alpha\rangle), \quad (8)$$

where $\mathcal{N}_\pm = \sqrt{2(1 \pm e^{-|\alpha|^2})} \simeq \sqrt{2}$ for $|\alpha| \gtrsim 4$ [54]. Alternatively, in the case of different frequency modes, $\omega_1 \neq \omega_2$, a maximally-entangled *NOON* state of the form

$$|\pm\Phi_{\text{NOON}}\rangle = \frac{1}{\mathcal{N}_\pm} (|0\alpha\rangle \pm |\alpha 0\rangle), \quad (9)$$

can be obtained by performing a π pulse to flip the qubit state right after turning on the first interaction and before the second one. The protocol would then require the following steps: (a) start modulating at $\omega_{\text{ac}} = \omega_1$, (b) turn off the interaction after time τ_1 , (c) apply π qubit pulse, and (d) switch on the second flux modulation with $\omega_{\text{ac}} = \omega_2$ for time $\tau_2 = \tau_1 \tilde{g}_1 / \tilde{g}_2$.

Additionally, more general ECS of the form,

$$|\Psi\rangle_{ij} = c_{00} |0_i 0_j\rangle + c_{1\alpha} |0_i \alpha_j\rangle + c_{\alpha 0} |\alpha_i 0_j\rangle + c_{\alpha\alpha} |\alpha_i \alpha_j\rangle, \quad (10)$$

with $c_{\alpha 0}, c_{0\alpha} \neq 0$, may also be generated using appropriately adjusted protocols. For example, starting from $|\psi\rangle_{\text{qij}} = |(0_q + 1_q)0_i 0_j\rangle$, then turning on the interaction with mode i for time τ_i such that $|\alpha| \equiv |\tilde{g}_i \tau_i| \gtrsim 4$, and applying a $R_{\hat{y} \frac{\pi}{2}}$ qubit pulse, results in the state $|\psi\rangle_{\text{qij}} = \frac{1}{2} [|0_q 0_i 0_j\rangle + |0_q \alpha_i 0_j\rangle + |1_q 0_i 0_j\rangle - |1_q \alpha_i 0_j\rangle]$. If we subsequently turn on the interaction with mode j (for time $\tau_j = \alpha / \tilde{g}_j$) and apply another $R_{\hat{y} \frac{\pi}{2}}$ qubit pulse, the resulting state is, $|\psi\rangle_{\text{qij}} = \frac{1}{\sqrt{2}} (|0\rangle_q |\Psi\rangle_{ij}^+ + |1\rangle_q |\Psi\rangle_{ij}^-)$, where

$$|\Psi\rangle_{ij}^\pm = \frac{1}{2} (|0_i 0_j\rangle + |0_i \alpha_j\rangle \pm |\alpha_i 0_j\rangle \mp |\alpha_i \alpha_j\rangle). \quad (11)$$

Finally, a strong measurement collapses the qubit in $|0\rangle_q$ or $|1\rangle_q$, projecting the system in the maximally-entangled two-mode state $|\Psi\rangle_{ij}^+$ or $|\Psi\rangle_{ij}^-$, respectively.

IV. NUMERICAL MODELING & BENCHMARKING

We benchmark the protocol described above for generating the Bell state $|\Psi_{\text{Bell}}\rangle$ against realistic experimental conditions including dissipation using the quantum statistical Lindblad master equation [55]

$$\begin{aligned} \dot{\rho} = & \frac{i}{\hbar} [\rho, \hat{H}] + \sum_j \frac{\omega_j}{Q_j} \left(n_j^{\text{th}} \mathcal{L}[\hat{a}_j^\dagger] \rho + (n_j^{\text{th}} + 1) \mathcal{L}[\hat{a}_j] \rho \right) \\ & + \frac{1}{T_1} \mathcal{L}[\hat{c}] \rho + \frac{1}{T_2} \mathcal{L}[\hat{c}^\dagger \hat{c}] \rho, \end{aligned} \quad (12)$$

where Q_j is the quality factor of each resonator, $\mathcal{L}[\hat{o}]\rho = (2\hat{o}\rho\hat{o}^\dagger - \hat{o}^\dagger\hat{o}\rho - \rho\hat{o}^\dagger\hat{o})/2$ are superoperators describing each bare dissipation channel and $n_j^{\text{th}} = 1/[\exp(\hbar\omega_j/(k_B T)) - 1]$ is the number of thermally excited magnons/phonons at temperature T . T_1 and T_2 are the qubit relaxation and dephasing times, respectively, for which we pick a realistic value of $50 \mu\text{s}$ throughout our simulations [6]. Of note, the in-plane

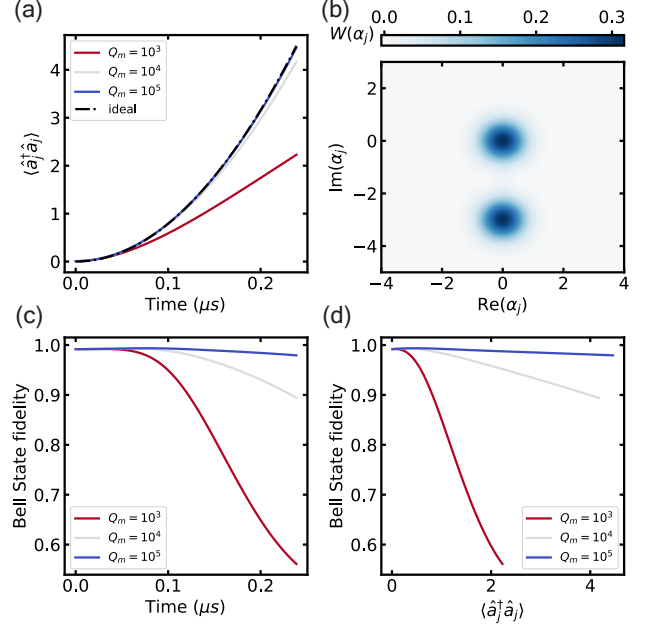


FIG. 2. Bell state benchmarking for the case of two Kittel modes in two identical YIG spheres, as schematically shown in Fig. 1(a). (a) Magnon number in each magnonic mode, as a function of time during the protocol, shown for different resonator quality factors. (b) Wigner function of the individual magnonic state in one mode, after tracing out the other mode, at the end of the protocol for $Q_m = 10^5$. The fidelity of the prepared state to the ideal Bell state $|\Psi_{\text{Bell}}\rangle$ is shown as a function of time in (c) and as a function of the magnon number in (d). System parameters: $\omega_{1,2}/(2\pi) = 1 \text{ GHz}$, $\tilde{g}_{1,2}/(2\pi) = 2 \text{ MHz}$, $T_1 = T_2 = 50 \mu\text{s}$, $T = 10 \text{ mK}$.

magnetic field that is required to enable the qubit coupling to the magnonic or the mechanical resonator, $B_z \sim 10 - 50 \text{ mT}$ [38, 39], is not expected to limit the qubit performance [56]. In addition, while the transmon is effectively a qubit, it is more accurately described as a three-level system with negative anharmonicity given by $\sim -E_C$. We therefore model it as such choosing a typical value of $E_C/h = 300 \text{ MHz}$ [6, 41].

We first study the case, schematically depicted in Fig. 1(a), of two YIG spheres placed diametrically opposite with respect to the center of the SQUID. For simplicity, we assume two identical spheres and Kittel modes with the same frequency, $\omega_{1,2}/(2\pi) = 1 \text{ GHz}$, as well as coupling to the qubit, $\tilde{g}_{1,2}/(2\pi) = 2 \text{ MHz}$, and study the performance of the protocol proposed above as a function of the resonator quality factor, Q_m , at $T = 10 \text{ mK}$ ($n_{1,2}^{\text{th}} \simeq 0.01$). For typical values of the Gilbert damping constant α_G we expect $Q_m = 1/\alpha_G \sim 10^3 - 10^5$ [45, 57, 58].

In Fig. 2(a) we plot the evolution of the magnon number in either mode j and compare it to the ideal case, i.e., without dissipation, where $\langle \hat{a}_j^\dagger \hat{a}_j \rangle(t) = |\tilde{g}_m t|^2/2$. In addition, in Fig. 2(b) we plot the Wigner quasi-probability

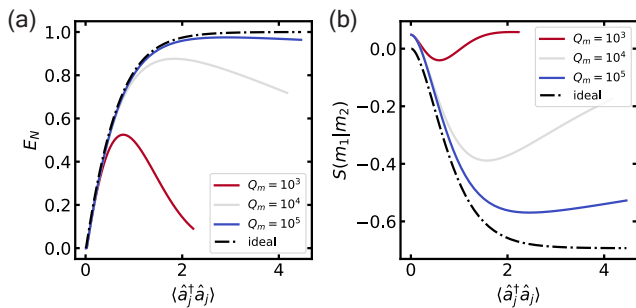


FIG. 3. (a) Logarithmic negativity and (b) conditional quantum entropy as a function of the magnon number for the magnon-magnon system described in Fig. 2. In the absence of dissipation (dashed-dotted curves) an ideal Bell state is created for magnon numbers $\langle \hat{a}_j^\dagger \hat{a}_j \rangle > 2$ with $E_N \rightarrow 1$ and $S(m_1|m_2) \rightarrow -\log 2$.

distribution at $t = 0.24 \mu\text{s}$ for $Q_m = 10^5$, which is defined as $W(\alpha_j) = 2/\pi \text{Tr} \left\{ D^\dagger(\alpha_j) \rho_j D(\alpha_j) e^{i\pi \hat{a}_j^\dagger \hat{a}_j} \right\}$, where $\rho_j \equiv \text{Tr}_i[\rho_{ij}]$ is the reduced density matrix of mode j and $D(\alpha_j) = e^{\alpha \hat{a}_j^\dagger - \alpha^* \hat{a}_j}$ is the displacement operator acting on this mode. The two-mode density matrix, ρ_{ij} , is obtained after projecting on $|+q\rangle$, and tracing out the qubit, i.e., $\rho_{ij} \equiv \text{Tr}_q[\rho | +q\rangle \langle +q|]$. We note that since we have two identical modes, the magnon number evolution as well as the reduced-state Wigner functions are exactly the same for both. Furthermore, Figs. 2(c) and 2(d) show the fidelity $\mathcal{F} = \sqrt{\langle +\Psi_{\text{Bell}} | \rho_{12} | +\Psi_{\text{Bell}} \rangle}$ [55, 59] of the prepared two-mode state to the ideal Bell state, as a function of time and magnon number, respectively. Evidently, for realistic values of the magnonic quality factors $Q_m \gtrsim 10^4$ [40, 57, 58], the desired Bell state can be prepared with high fidelity $\mathcal{F} \lesssim 90\%$.

To showcase the evolution of the bipartite entanglement during the protocol, in Fig. 3(a) we plot the logarithmic negativity $E_N = \log_2(2N(\rho_{12})+1)$, where $N(\rho_{12})$ is the sum of negative eigenvalues of the partial transpose of the two-mode density matrix ρ_{12} [60]. The dashed-dotted curve shows the logarithmic negativity evolution in the ideal case, $E_N(t) = \log_2 \left[2/(e^{-|\tilde{g}_j t|^2} + 1) \right]$ [61]. For $|\alpha| \equiv |\tilde{g}_j t| \gtrsim 2$ it approaches the ideal value of $E_N^{\text{max}} = 1$, where the two modes are maximally entangled, before magnon dissipation eventually takes over and the entanglement gets lost.

Furthermore, in Fig. 3(b) we plot the conditional quantum entropy $S(m_1|m_2) = S(\rho_{12}) - S(\rho_2)$ [62, 63], where $S(\rho_{ij})$ and $S(\rho_j)$ are the Von Neumann entropies of the joint and reduced state, respectively, with $S(\rho) = -\text{Tr}[\rho \ln \rho]$. Negative conditional quantum entropy serves as a sufficient criterion for the quantum state to be entangled and provides a measure of the degree of coherent quantum communication between the two entangled modes [62, 63]. For maximally-entangled Bell

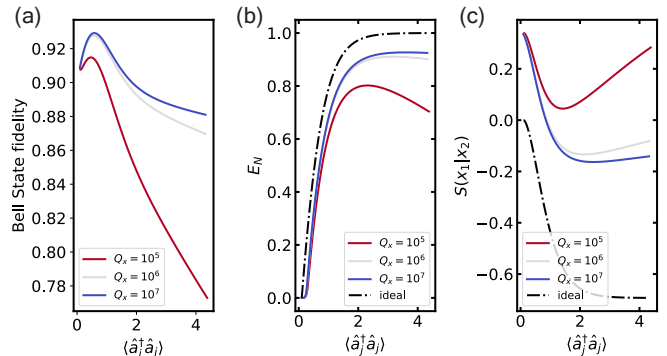


FIG. 4. (a) Bell state fidelity, (b) logarithmic negativity and (c) conditional quantum entropy as a function of the phonon number for the case of two SQUID-embedded mechanical nanobeams interacting via the transmon. System parameters: $\omega_{1,2}/(2\pi) = 10$ MHz, $\tilde{g}_{1,2}/(2\pi) = 100$ kHz, $T_1 = T_2 = 50 \mu\text{s}$, $T = 10$ mK, initial $n_{1,2}^{\text{th}} = 0.1$.

states we have $S(\rho_{ij}) = 0$ and $S(\rho_j) = \ln 2$. Therefore, in the limit of large magnon numbers, we expect $S(m_1|m_2) \rightarrow -\ln 2$, as illustrated by the dashed-dotted curve plotting the ideal (dissipationless) case. However, as the entanglement starts decreasing due to magnon dissipation, the joint entropy of the system becomes positive and both $S(\rho_{ij})$ and $S(\rho_i)$ start increasing. Therefore, as expected, the positive value threshold for $S(m_1|m_2)$ is surpassed faster and at lower magnon numbers as the quality factors get smaller. Note that initially $S(m_1|m_2) > 0$ due to the fact that the modes start in a thermal state with $n_{\text{th}} \simeq 0.01$.

The protocol described above can also be applied to entangle mechanical beam resonators embedded in the SQUID loop, as depicted in Fig. 1(b). These can be realized using carbon nanotubes [40] or aluminum-based mechanical beams [29–31, 39] interacting via radiation-pressure couplings with the transmon. The former have operating frequencies and quality factors similar to the magnonic case studied above, therefore, the results in Figs. 2 and 3 are applicable as well. On the other hand, mechanical beam resonators made of aluminum typically operate in the range 1 – 10 MHz, with quality factors $Q_x \gtrsim 10^5$ [29–31].

Therefore, in conjunction with the magnonic case, we numerically test the same protocol for creating mechanical Bell states between two SQUID-embedded aluminum beam resonator modes [30], with the same frequency $\omega_{1,2}/(2\pi) = 10$ MHz and coupling to the qubit $\tilde{g}_{1,2}/(2\pi) = 100$ kHz. Typical temperatures of $T \sim 10$ mK, correspond to high thermal population at these frequencies, however, cooling schemes can reduce the number of thermal phonons to $\lesssim 0.1$ [39, 40]. We therefore assume an attainable initial thermal population $n_{1,2}^{\text{th}} = 0.1$ and an operating temperature of $T = 10$ mK.

In Figs. 4(a) and 4(b) we plot the Bell-state fidelity and the logarithmic negativity, respectively, as a function of

the phonon number during the protocol for quality factors in the range $Q_x = 10^5 - 10^7$. Note that initially the fidelity is less than 1, due to the finite thermal population in both resonators, however, as the protocol evolves it starts increasing before phonon dissipation takes over. We find that, for realistic quality factors $Q_x \gtrsim 10^6$, high phonon number Bell-states can be prepared with high fidelity and sufficiently high entanglement as quantified by E_N . However, as shown in Fig. 4(c), the effects of the initial thermal population seem to be detrimental to the conditional quantum entropy $S(x_1|x_2)$ which remains far from the ideal limit during the whole protocol and only reaches negative values for $Q_j \sim 10^6$.

Experimental verification of the prepared states can be obtained by performing state tomography. For example, in the case of mechanical resonators, by sideband driving on the qubit one may engineer beam-splitter and two-mode squeezing interactions that can be used to detect correlations of the entangled state similar to Ref. [26]. This method may also be applied to the magnonic resonators, for which independent state tomography techniques exist as well [64]. However, strong driving may severely impact the qubit state [65] limiting the success of such protocols. For this reason we have also analyzed an alternative scheme for reading out the entangled states, presented in the Appendix, which relies solely on switching on/off the interaction and performing magnon/phonon displacements and qubit measurements.

V. CONCLUSION

In summary, we have proposed a scheme for generating ECS of magnons/phonons in a hybrid circuit QED architecture comprising a superconducting transmon qubit coupled to different magnonic/mechanical modes via bipartite flux-mediated interactions. In particular, we have highlighted several schemes for creating maximally-entangled states and, as a proof-of-principle demonstration, we have numerically tested a simple protocol for generating magnonic and mechanical Bell states under realistic experimental conditions. We show that high-fidelity Bell states can be prepared in the presence of typical dissipation mechanisms in the system. Furthermore, in the Appendix we have analyzed a readout scheme, using standard circuit operations, that can be used as an alternative to existing tomography methods for verifying the prepared states. Our results pave the way towards creating controllable quantum networks of entangled magnons in a flexible and scalable platform without relying on microwave 3D cavities or strong driving. Although for simplicity

we have considered identical YIG spheres, our results are also applicable to nonidentical modes and other geometries such as micro-disk resonators [66]. Finally, as we demonstrate numerically, the proposed scheme for creating and controlling ECS is also applicable to SQUID-embedded mechanical beam resonators, opening up new opportunities for quantum information tasks in this platform and potentially giving rise to novel magnonic-mechanical hybrid devices.

ACKNOWLEDGMENTS

We thank Sanchar Sharma and Victor Bittencourt for helpful discussions. This research was supported by the Dutch Foundation for Scientific Research (NWO). M.K. and S.V.K. would like to acknowledge financial support by the German Federal Ministry of Education and Research (BMBF) project QECHQS (Grant No. 16KIS1590K).

APPENDIX: READOUT SCHEME

We now describe a method for reading out the two-mode ECS discussed in the main text, using only qubit measurements and displacement operations on the bosonic modes. We start with the assumption that the most general state one can prepare with the system Hamiltonian in Eq. (6) is of the following form,

$$|\Psi\rangle_{ij} = c_0 e^{i\theta_0} |0_i 0_j\rangle + c_1 e^{i\theta_1} |0_i \alpha_j\rangle + c_2 e^{i\theta_2} |\alpha_i 0_j\rangle + c_3 e^{i\theta_3} |\alpha_i \alpha_j\rangle, \quad (\text{A13})$$

where c_j are real positive numbers and $\sum_{j=0}^3 c_j^2 = 1$. Our assumption is based on the fact that the engineered radiation-pressure interaction in Eq. (6) can only lead to magnon/phonon displacements when the qubit is in the excited state, therefore, for the protocols described in the main text, where the interaction is activated at least once for each bosonic mode, Eq. (A13) describes the mode general state one can prepare. In addition, single-photon losses acting on coherent states result in a coherent state of smaller amplitude, therefore this decay channel does not alter the form of the state described in Eq. (A13).

Assuming the state in Eq. (A13) has been prepared, we start the readout protocol by preparing the qubit in a general superposition state $|\phi\rangle_{\text{q}} = (|0\rangle_{\text{q}} + e^{i\phi} |1\rangle_{\text{q}})/\sqrt{2}$. After switching on both interactions, the system wavefunction evolves as

$$U_{\text{int}}^{(i)} U_{\text{int}}^{(j)} |\phi\rangle_{\text{q}} |\Psi\rangle_{\text{ij}} = \frac{1}{\sqrt{2}} \left[|0\rangle_{\text{q}} (c_0 e^{i\theta_0} |0_i 0_j\rangle + c_1 e^{i\theta_1} |0_i \alpha_j\rangle + c_2 e^{i\theta_2} |\alpha_i 0_j\rangle + c_3 e^{i\theta_3} |\alpha_i \alpha_j\rangle) + |1\rangle_{\text{q}} e^{i(\phi+\bar{\phi})} (c_0 e^{i\theta_0} |\beta_i \beta_j\rangle + c_1 e^{i\theta_1+\gamma_j} |\beta_i(\alpha+\beta)_j\rangle + c_2 e^{i\theta_2+\gamma_i} |(\alpha+\beta)_i \beta_j\rangle + c_3 e^{i\theta_3+\gamma_i+\gamma_j} |(\alpha+\beta)_i(\alpha+\beta)_j\rangle) \right], \quad (\text{A14})$$

where $U_{\text{int}}^{(j)} = \exp\left\{i\tilde{g}_j \hat{c}^\dagger \hat{c}(\hat{a}_j e^{i\theta} + \hat{a}_j^\dagger e^{-i\theta})t\right\}$.

The displacement amplitudes and corresponding geometric phases, which arise from the radiation pressure interactions, are given by $\beta_{i,j} \doteq \frac{\beta(t_{i,j})}{\omega_{i,j}}$ ($e^{i\omega_{i,j}t_{i,j}} - 1$) and $\phi \doteq \bar{\phi}(t_{i,j}) = (g_{i,j}/\omega_{i,j})^2 (\omega_{i,j}t_{i,j} - \sin(\omega_{i,j}t_{i,j}))$ [38, 67]. For simplification purposes we have assumed that the latter are equal and, since ϕ is arbitrarily determined at the qubit preparation stage, they can be absorbed into a redefinition of $\phi \rightarrow \bar{\phi} + \phi$. The phases $\gamma_{i,j} = \text{Im}(\alpha^* \beta_{i,j})$ arise from

the fact that in general two consecutive displacements do not commute.

The above state can also be written as

$$|\psi\rangle_{\text{qij}} = \frac{1}{2} \left(|+\rangle_{\text{q}} |\Psi^+\rangle_{\text{ij}} + |-\rangle_{\text{q}} |\Psi^-\rangle_{\text{ij}} \right), \quad (\text{A15})$$

where $|\pm\rangle = (|0\rangle \pm |1\rangle)/\sqrt{2}$ are the eigenstates of the Pauli $\hat{\sigma}_x$ operator and

$$|\Psi^\pm\rangle_{\text{ij}} = c_0 e^{i\theta_0} |0_i 0_j\rangle + c_1 e^{i\theta_1} |0_i \alpha_j\rangle + c_2 e^{i\theta_2} |\alpha_i 0_j\rangle + c_3 e^{i\theta_3} |\alpha_i \alpha_j\rangle \pm \left(c_0 e^{i\theta_0+\phi} |\beta_i \beta_j\rangle + c_1 e^{i\theta_1+\phi+\gamma} |\beta_i(\alpha+\beta)_j\rangle + c_2 e^{i\theta_2+\phi+\gamma} |(\alpha+\beta)_i \beta_j\rangle + c_3 e^{i\theta_3+\phi+2\gamma} |(\alpha+\beta)_i(\alpha+\beta)_j\rangle \right). \quad (\text{A16})$$

The expectation value of the qubit in the $|\pm\rangle$ basis is

then given by

$$\langle \hat{\sigma}_x \rangle_{\beta,\beta} = \frac{1}{4} \left(|\langle \Psi^+_{\text{ij}} | \Psi^+_{\text{ij}} \rangle|^2 - |\langle \Psi^-_{\text{ij}} | \Psi^-_{\text{ij}} \rangle|^2 \right). \quad (\text{A17})$$

We now consider several cases for each displacement:

(I) First, assuming the coupling strength and interaction times for both resonators are chosen such that $\beta_{i,j} = \alpha_{i,j}$, we have ($\gamma_{i,j} = 0$):

$$|\Psi^\pm\rangle_{\text{ij}} = c_0 e^{i\theta_0} |0_i 0_j\rangle + c_1 e^{i\theta_1} |0_i \alpha_j\rangle + c_2 e^{i\theta_2} |\alpha_i 0_j\rangle + (c_3 e^{i\theta_3} \pm c_0 e^{i\theta_0+\phi}) |\alpha_i \alpha_j\rangle \pm c_1 e^{i\theta_1+\phi} |\alpha_i (2\alpha)_j\rangle \pm c_2 e^{i\theta_2+\phi} |(2\alpha)_i \alpha_j\rangle \pm c_3 e^{i\theta_3+\phi} |(2\alpha)_i (2\alpha)_j\rangle \quad (\text{A18})$$

From Eq. (A17) we obtain

$$\langle \hat{\sigma}_x \rangle_{\alpha,\alpha} = |c_3 e^{i\theta_3} + c_0 e^{i\theta_0+\phi}|^2 - |c_3 e^{i\theta_3} - c_0 e^{i\theta_0+\phi}|^2 = c_0 c_3 \cos(\phi + \theta_0 - \theta_3). \quad (\text{A19})$$

Additionally, for $\beta_{i,j} = -\alpha_{i,j}$ it can be shown that

$$\langle \hat{\sigma}_x \rangle_{-\alpha,-\alpha} = c_0 c_3 \cos(\phi + \theta_3 - \theta_0). \quad (\text{A20})$$

(II) For the case $\beta_i = \alpha_i$, $\beta_j = -\alpha_j$, using Eq. (A16)

and Eq. (A17), it follows that

$$\langle \hat{\sigma}_x \rangle_{\alpha,-\alpha} = c_1 c_2 \cos(\phi + \theta_1 - \theta_2). \quad (\text{A21})$$

Similarly for $\beta_i = -\alpha_i$, $\beta_j = \alpha_j$ we obtain

$$\langle \hat{\sigma}_x \rangle_{-\alpha,\alpha} = c_1 c_2 \cos(\phi + \theta_2 - \theta_1) \quad (\text{A22})$$

(III) For the cases $\beta_i = \alpha_i$, $\beta_j = 0$ and $\beta_i = -\alpha_i$, $\beta_j = 0$ we have

$$\langle \hat{\sigma}_x \rangle_{\alpha,0} = c_0 c_2 \cos(\phi + \theta_0 - \theta_2) + c_1 c_3 \cos(\phi + \theta_1 - \theta_3) \quad (\text{A23})$$

and

$$\langle \hat{\sigma}_x \rangle_{-\alpha,0} = c_0 c_2 \cos(\phi + \theta_2 - \theta_0) + c_1 c_3 \cos(\phi + \theta_3 - \theta_1) \quad (\text{A24})$$

respectively.

(IV) For $\beta_i = 0$, $\beta_j = \alpha_i$ and $\beta_i = 0$, $\beta_j = -\alpha_i$ we find two more equations,

$$\langle \hat{\sigma}_x \rangle_{0,\alpha} = c_0 c_1 \cos(\phi + \theta_0 - \theta_1) + c_2 c_3 \cos(\phi + \theta_2 - \theta_3). \quad (\text{A25})$$

and

$$\langle \hat{\sigma}_x \rangle_{0,-\alpha} = c_0 c_1 \cos(\phi + \theta_1 - \theta_0) + c_2 c_3 \cos(\phi + \theta_3 - \theta_2) \quad (\text{A26})$$

Finally for $\beta_{i,j} = 0$ we obtain the following relation

$$\langle \hat{\sigma}_x \rangle_{0,0} = (c_0^2 + c_1^2 + c_2^2 + c_3^2) \cos \phi, \quad (\text{A27})$$

which is equivalent to the normalisation condition for $|\Psi\rangle_{ij}$ with the additional degree of freedom ϕ .

The above equations are not yet in a form where they can be used to obtain all pairs of c_i, θ_i straightforwardly. However, they can be combined and further simplified using basic trigonometric relations as shown below:

(i) First, adding and subtracting equations (A19) and (A20) we obtain

$$\langle \hat{\sigma}_x \rangle_{\alpha,\alpha} + \langle \hat{\sigma}_x \rangle_{-\alpha,-\alpha} = 2c_0 c_3 \cos \phi \cos(\theta_3 - \theta_0), \quad (\text{A28})$$

and

$$\langle \hat{\sigma}_x \rangle_{\alpha,\alpha} - \langle \hat{\sigma}_x \rangle_{-\alpha,-\alpha} = 2c_0 c_3 \sin \phi \sin(\theta_3 - \theta_0). \quad (\text{A29})$$

If the qubit is prepared such that $\phi = \pi/4$ then by combining the above two equations we obtain a relation for c_0, c_3 that does not depend on θ_0, θ_3 :

$$c_0 c_3 = \sqrt{|\langle \hat{\sigma}_x \rangle_{\alpha,\alpha}|^2 + |\langle \hat{\sigma}_x \rangle_{-\alpha,-\alpha}|^2}. \quad (\text{A30})$$

If $c_0 c_3 \neq 0$ we can also determine the phases. First, $e^{i\theta_0}$ in Eq. (A13) can be absorbed into a global phase factor multiplying $|\Psi\rangle_{ij}$ followed by a redefinition of $\theta_{1,2,3} \rightarrow \theta_{1,2,3}/\theta_0$ (equivalent to defining $\theta_0 = 0$ or 2π). Then for $\phi = \pi/4$ we have

$$\theta_3 = \arctan \left(\frac{\langle \hat{\sigma}_x \rangle_{\alpha,\alpha} - \langle \hat{\sigma}_x \rangle_{-\alpha,-\alpha}}{\langle \hat{\sigma}_x \rangle_{\alpha,\alpha} + \langle \hat{\sigma}_x \rangle_{-\alpha,-\alpha}} \right). \quad (\text{A31})$$

(ii) Following the same recipe we can obtain similar relations for c_1, c_2 and θ_1, θ_2 . In this case, by combining equations (A21) and (A22) for $\phi = \pi/4$ we obtain the following equations

$$c_1 c_2 = \sqrt{|\langle \hat{\sigma}_x \rangle_{\alpha,-\alpha}|^2 + |\langle \hat{\sigma}_x \rangle_{-\alpha,\alpha}|^2}, \quad (\text{A32})$$

and (assuming $c_1 c_2 \neq 0$)

$$\theta_2 - \theta_1 = \arctan \left(\frac{\langle \hat{\sigma}_x \rangle_{\alpha,-\alpha} - \langle \hat{\sigma}_x \rangle_{-\alpha,\alpha}}{\langle \hat{\sigma}_x \rangle_{\alpha,-\alpha} + \langle \hat{\sigma}_x \rangle_{-\alpha,\alpha}} \right). \quad (\text{A33})$$

(iii) Furthermore, from equations (A23) and (A24) we obtain (for $\phi = \pi/4$)

$$\begin{aligned} & (\langle \hat{\sigma}_x \rangle_{\alpha,0} + \langle \hat{\sigma}_x \rangle_{-\alpha,0})^2 \pm (\langle \hat{\sigma}_x \rangle_{\alpha,0} - \langle \hat{\sigma}_x \rangle_{-\alpha,0})^2 \\ &= 2 [(c_0 c_2)^2 + (c_1 c_3)^2 + 2c_0 c_1 c_2 c_3 \cos(\theta_2 \pm \theta_1 \mp \theta_3)]. \end{aligned} \quad (\text{A34})$$

Using equations (A30), (A31), (A32) and (A33) we can obtain a relation for c_0, c_1, c_2, c_3 with no dependence on the phases:

$$\begin{aligned} (c_0 c_2)^2 + (c_1 c_3)^2 &= f(\langle \hat{\sigma}_x \rangle_{\alpha,0}, \langle \hat{\sigma}_x \rangle_{-\alpha,0}, \langle \hat{\sigma}_x \rangle_{\alpha,\alpha}, \langle \hat{\sigma}_x \rangle_{-\alpha,-\alpha}, \langle \hat{\sigma}_x \rangle_{\alpha,-\alpha}, \langle \hat{\sigma}_x \rangle_{-\alpha,\alpha}) \\ &= 2 \langle \hat{\sigma}_x \rangle_{\alpha,0} \langle \hat{\sigma}_x \rangle_{-\alpha,0} - 2 \left[\sqrt{(|\langle \hat{\sigma}_x \rangle_{\alpha,\alpha}|^2 + |\langle \hat{\sigma}_x \rangle_{-\alpha,-\alpha}|^2)(|\langle \hat{\sigma}_x \rangle_{\alpha,-\alpha}|^2 + |\langle \hat{\sigma}_x \rangle_{-\alpha,\alpha}|^2)} \right. \\ &\quad \left. \times \cos \left(\arctan \left(\frac{\langle \hat{\sigma}_x \rangle_{\alpha,\alpha} - \langle \hat{\sigma}_x \rangle_{-\alpha,-\alpha}}{\langle \hat{\sigma}_x \rangle_{\alpha,\alpha} + \langle \hat{\sigma}_x \rangle_{-\alpha,-\alpha}} \right) + \arctan \left(\frac{\langle \hat{\sigma}_x \rangle_{\alpha,-\alpha} - \langle \hat{\sigma}_x \rangle_{-\alpha,\alpha}}{\langle \hat{\sigma}_x \rangle_{\alpha,-\alpha} + \langle \hat{\sigma}_x \rangle_{-\alpha,\alpha}} \right) \right) \right]. \end{aligned} \quad (\text{A35})$$

(iv) Similarly, from equations (A25) and (A26) we ob-

tain (for $\phi = \pi/4$)

$$\begin{aligned} & (\langle \hat{\sigma}_x \rangle_{0,\alpha} + \langle \hat{\sigma}_x \rangle_{0,-\alpha})^2 \pm (\langle \hat{\sigma}_x \rangle_{0,\alpha} - \langle \hat{\sigma}_x \rangle_{0,-\alpha})^2 \\ &= 2 [(c_0 c_1)^2 + (c_2 c_3)^2 + 2c_0 c_1 c_2 c_3 \cos(\theta_1 \pm \theta_2 \mp \theta_3)]. \end{aligned} \quad (\text{A36})$$

Again, using equations (A30), (A31), (A32) and (A33) we can obtain another relation for c_0, c_1, c_2, c_3 with no dependence on the phases:

$$\begin{aligned}
(c_0 c_1)^2 + (c_2 c_3)^2 &= g(\langle \hat{\sigma}_x \rangle_{0,\alpha}, \langle \hat{\sigma}_x \rangle_{0,-\alpha}, \langle \hat{\sigma}_x \rangle_{\alpha,\alpha}, \langle \hat{\sigma}_x \rangle_{-\alpha,-\alpha}, \langle \hat{\sigma}_x \rangle_{\alpha,-\alpha}, \langle \hat{\sigma}_x \rangle_{-\alpha,\alpha}) \\
&= 2\langle \hat{\sigma}_x \rangle_{0,\alpha} \langle \hat{\sigma}_x \rangle_{0,-\alpha} - 2 \left[\sqrt{(|\langle \hat{\sigma}_x \rangle_{\alpha,\alpha}|^2 + |\langle \hat{\sigma}_x \rangle_{-\alpha,-\alpha}|^2)(|\langle \hat{\sigma}_x \rangle_{\alpha,-\alpha}|^2 + |\langle \hat{\sigma}_x \rangle_{-\alpha,\alpha}|^2)} \right. \\
&\quad \left. \times \cos \left(\arctan \left(\frac{\langle \hat{\sigma}_x \rangle_{\alpha,\alpha} - \langle \hat{\sigma}_x \rangle_{-\alpha,-\alpha}}{\langle \hat{\sigma}_x \rangle_{\alpha,\alpha} + \langle \hat{\sigma}_x \rangle_{-\alpha,-\alpha}} \right) - \arctan \left(\frac{\langle \hat{\sigma}_x \rangle_{\alpha,-\alpha} - \langle \hat{\sigma}_x \rangle_{-\alpha,\alpha}}{\langle \hat{\sigma}_x \rangle_{\alpha,-\alpha} + \langle \hat{\sigma}_x \rangle_{-\alpha,\alpha}} \right) \right) \right]. \quad (\text{A37})
\end{aligned}$$

In our case we are interested in reading out the Bell state

$$|\Psi\rangle_{ij} = \frac{1}{\sqrt{N}} (|0_i 0_j\rangle + e^{i\theta} |\alpha_i \alpha_j\rangle), \quad (\text{A38})$$

i.e. the state in Eq. (A13) with $\theta_3 = \theta$, $c_0 = c_3 = \frac{1}{\sqrt{N}}$ and $c_1 = c_2 = 0$. Let us assume that we have prepared the general state in Eq. (A13). First, we can measure $\langle \hat{\sigma}_x \rangle_{\alpha,\alpha}$ and $\langle \hat{\sigma}_x \rangle_{-\alpha,-\alpha}$ and from Eq. (A30) determine $c_0 c_3$. If we have indeed prepared the target state shown in Eq. (A38) then this product should be nonzero. Then we proceed

by measuring $\langle \hat{\sigma}_x \rangle_{\alpha,-\alpha}$ and $\langle \hat{\sigma}_x \rangle_{-\alpha,\alpha}$ which should both be zero indicating that either $c_1 = 0$ or $c_2 = 0$ according to Eq. (A32). Additionally equations (A35) and (A37) should also equate to zero indicating $c_1 = c_2 = 0$. Finally, combining equations (A27) and (A30) we have

$$(c_0 - c_3)^2 = \sqrt{2} \langle \hat{\sigma}_x \rangle_{0,0} - 2 \sqrt{(|\langle \hat{\sigma}_x \rangle_{\alpha,\alpha}|^2 + |\langle \hat{\sigma}_x \rangle_{-\alpha,-\alpha}|^2)}. \quad (\text{A39})$$

If indeed the state in Eq. (A38) is prepared then we should find that $\langle \hat{\sigma}_x \rangle_{0,0} = \sqrt{2}(|\langle \hat{\sigma}_x \rangle_{\alpha,\alpha}|^2 + |\langle \hat{\sigma}_x \rangle_{-\alpha,-\alpha}|^2)$, and therefore $c_0 = c_3 = (|\langle \hat{\sigma}_x \rangle_{\alpha,\alpha}|^2 + |\langle \hat{\sigma}_x \rangle_{-\alpha,-\alpha}|^2)^{1/4} = 2^{-1/4} \langle \hat{\sigma}_x \rangle_{0,0}$.

* marios.kounalakis@gmail.com

- ¹ A. G. J. MacFarlane, J. P. Dowling, and G. J. Milburn, *Philosophical Transactions of the Royal Society of London. Series A: Mathematical, Physical and Engineering Sciences* **361**, 1655 (2003).
- ² A. Acín, I. Bloch, H. Buhrman, T. Calarco, C. Eichler, J. Eisert, D. Esteve, N. Gisin, S. J. Glaser, F. Jelezko, S. Kuhr, M. Lewenstein, M. F. Riedel, P. O. Schmidt, R. Thew, A. Wallraff, I. Walmsley, and F. K. Wilhelm, *New Journal of Physics* **20**, 080201 (2018).
- ³ G. Kurizki, P. Bertet, Y. Kubo, K. Mølmer, D. Petrosyan, P. Rabl, and J. Schmiedmayer, *Proceedings of the National Academy of Sciences* **112**, 3866 (2015).
- ⁴ A. Clerk, K. Lehnert, P. Bertet, J. Petta, and Y. Nakamura, *Nature Physics* **16**, 257 (2020).
- ⁵ M. Devoret and R. Schoelkopf, *Science* **339**, 1169 (2013).
- ⁶ M. Kjaergaard, M. E. Schwartz, J. Braumüller, P. Krantz, J. I.-J. Wang, S. Gustavsson, and W. D. Oliver, *Annual Review of Condensed Matter Physics* **11**, 369 (2020).
- ⁷ M. Aspelmeyer, T. J. Kippenberg, and F. Marquardt, *Rev. Mod. Phys.* **86**, 1391 (2014).
- ⁸ T. Yu, Y.-X. Zhang, S. Sharma, X. Zhang, Y. M. Blanter, and G. E. W. Bauer, *Phys. Rev. Lett.* **124**, 107202 (2020).
- ⁹ I. Bertelli, J. J. Carmiggelt, T. Yu, B. G. Simon, C. C. Pothoven, G. E. W. Bauer, Y. M. Blanter, J. Aarts, and T. van der Sar, *Science Advances* **6**, eabd3556 (2020).
- ¹⁰ D. Lachance-Quirion, Y. Tabuchi, A. Gloppe, K. Usami, and Y. Nakamura, *Applied Physics Express* **12**, 070101 (2019).
- ¹¹ H. Yuan, Y. Cao, A. Kamra, R. A. Duine, and P. Yan, *Physics Reports* **965**, 1 (2022), quantum magnonics: When magnon spintronics meets quantum information science.
- ¹² B. Yurke and D. Stoler, *Phys. Rev. Lett.* **57**, 13 (1986).

- ¹³ B. C. Sanders, *Journal of Physics A: Mathematical and Theoretical* **45**, 244002 (2012).
- ¹⁴ S. J. van Enk and O. Hirota, *Phys. Rev. A* **64**, 022313 (2001).
- ¹⁵ X. Wang, *Phys. Rev. A* **64**, 022302 (2001).
- ¹⁶ P. T. Cochrane, G. J. Milburn, and W. J. Munro, *Phys. Rev. A* **59**, 2631 (1999).
- ¹⁷ M. C. de Oliveira and W. J. Munro, *Phys. Rev. A* **61**, 042309 (2000).
- ¹⁸ H. Jeong and M. S. Kim, *Phys. Rev. A* **65**, 042305 (2002).
- ¹⁹ P. van Loock, W. J. Munro, K. Nemoto, T. P. Spiller, T. D. Ladd, S. L. Braunstein, and G. J. Milburn, *Phys. Rev. A* **78**, 022303 (2008).
- ²⁰ A. E. Allati, Y. Hassouni, and N. Metwally, *Physica Scripta* **83**, 065002 (2011).
- ²¹ W. J. Munro, K. Nemoto, G. J. Milburn, and S. L. Braunstein, *Phys. Rev. A* **66**, 023819 (2002).
- ²² J. Joo, W. J. Munro, and T. P. Spiller, *Phys. Rev. Lett.* **107**, 083601 (2011).
- ²³ L. Diósi, *Journal of Physics: Conference Series* **306**, 012006 (2011).
- ²⁴ D. Kafri, J. M. Taylor, and G. J. Milburn, *New Journal of Physics* **16**, 065020 (2014).
- ²⁵ C. Ockeloen-Korppi, E. Damskägg, J.-M. Pirkkalainen, M. Asjad, A. Clerk, F. Massel, M. Woolley, and M. Silanpää, *Nature* **556**, 478 (2018).
- ²⁶ S. Kotler, G. A. Peterson, E. Shojaei, F. Lecocq, K. Cicak, A. Kwiatkowski, S. Geller, S. Glancy, E. Knill, R. W. Simmonds, J. Aumentado, and J. D. Teufel, *Science* **372**, 622 (2021).
- ²⁷ R. Riedinger, A. Wallucks, I. Marinković, C. Löschner, M. Aspelmeyer, S. Hong, and S. Gröblacher, *Nature* **556**, 473 (2018).

- ²⁸ E. A. Wollack, A. Y. Cleland, R. G. Gruenke, Z. Wang, P. Arrangoiz-Arriola, and A. H. Safavi-Naeini, *Nature* **604**, 463 (2022).
- ²⁹ I. Rodrigues, D. Bothner, and G. Steele, *Nature communications* **10**, 5359 (2019).
- ³⁰ P. Schmidt, M. T. Amawi, S. Pogorzalek, F. Deppe, A. Marx, R. Gross, and H. Huebl, *Communications Physics* **3**, 1 (2020).
- ³¹ T. Bera, S. Majumder, S. K. Sahu, and V. Singh, *Communications Physics* **4**, 1 (2021).
- ³² J. Simon, H. Tanji, S. Ghosh, and V. Vuletić, *Nature Physics* **3**, 765 (2007).
- ³³ Z. Zhang, M. O. Scully, and G. S. Agarwal, *Phys. Rev. Res.* **1**, 023021 (2019).
- ³⁴ J. Li and S.-Y. Zhu, *New Journal of Physics* **21**, 085001 (2019).
- ³⁵ X. Zhang, C.-L. Zou, L. Jiang, and H. X. Tang, *Science Advances* **2**, e1501286 (2016).
- ³⁶ J. M. P. Nair and G. S. Agarwal, *Applied Physics Letters* **117**, 084001 (2020).
- ³⁷ M. Yu, S.-Y. Zhu, and J. Li, *Journal of Physics B: Atomic, Molecular and Optical Physics* **53**, 065402 (2020).
- ³⁸ M. Kounalakis, G. E. W. Bauer, and Y. M. Blanter, *Phys. Rev. Lett.* **129**, 037205 (2022).
- ³⁹ M. Kounalakis, Y. M. Blanter, and G. A. Steele, *Phys. Rev. Research* **2**, 023335 (2020).
- ⁴⁰ K. E. Khosla, M. R. Vanner, N. Ares, and E. A. Laird, *Phys. Rev. X* **8**, 021052 (2018).
- ⁴¹ J. Koch, T. M. Yu, J. Gambetta, A. A. Houck, D. I. Schuster, J. Majer, A. Blais, M. H. Devoret, S. M. Girvin, and R. J. Schoelkopf, *Phys. Rev. A* **76**, 042319 (2007).
- ⁴² U. Vool and M. Devoret, *International Journal of Circuit Theory and Applications* **45**, 897 (2017).
- ⁴³ H. Yuan, J. Xie, and R. A. Duine, arXiv preprint arXiv:2301.09095 (2023).
- ⁴⁴ Y. Tabuchi, S. Ishino, A. Noguchi, T. Ishikawa, R. Yamazaki, K. Usami, and Y. Nakamura, *Comptes Rendus Physique* **17**, 729 (2016).
- ⁴⁵ B. Zare Rameshti, S. Viola Kusminskiy, J. A. Haigh, K. Usami, D. Lachance-Quirion, Y. Nakamura, C.-M. Hu, H. X. Tang, G. E. Bauer, and Y. M. Blanter, *Physics Reports* **979**, 1 (2022).
- ⁴⁶ D. D. Stancil and A. Prabhakar, *Spin waves*, Vol. 5 (Springer, 2009).
- ⁴⁷ S. Sharma, *Cavity optomagnonics: Manipulating magnetism by light*, Ph.D. thesis, Delft University of Technology (2019).
- ⁴⁸ M. Kounalakis, Y. M. Blanter, and G. A. Steele, *npj Quantum Information* **5**, 100 (2019).
- ⁴⁹ A. Nunnenkamp, K. Børkje, and S. M. Girvin, *Phys. Rev. Lett.* **107**, 063602 (2011).
- ⁵⁰ P. D. Nation, J. Suh, and M. P. Blencowe, *Phys. Rev. A* **93**, 022510 (2016).
- ⁵¹ L. Tian, *Phys. Rev. B* **72**, 195411 (2005).
- ⁵² D. Kielpinski, D. Kafri, M. J. Woolley, G. J. Milburn, and J. M. Taylor, *Phys. Rev. Lett.* **108**, 130504 (2012).
- ⁵³ M. Mirrahimi, Z. Leghtas, V. V. Albert, S. Touzard, R. J. Schoelkopf, L. Jiang, and M. H. Devoret, *New Journal of Physics* **16**, 045014 (2014).
- ⁵⁴ T. C. Ralph, A. Gilchrist, G. J. Milburn, W. J. Munro, and S. Glancy, *Phys. Rev. A* **68**, 042319 (2003).
- ⁵⁵ J. Johansson, P. Nation, and F. Nori, *Computer Physics Communications* **183**, 1760 (2012).
- ⁵⁶ J. Krause, C. Dickel, E. Vaal, M. Vielmetter, J. Feng, R. Bounds, G. Catelani, J. M. Fink, and Y. Ando, *Phys. Rev. Applied* **17**, 034032 (2022).
- ⁵⁷ Y. Tabuchi, S. Ishino, A. Noguchi, T. Ishikawa, R. Yamazaki, K. Usami, and Y. Nakamura, *Science* **349**, 405 (2015).
- ⁵⁸ S. Klingler, H. Maier-Flaig, C. Dubs, O. Surzhenko, R. Gross, H. Huebl, S. T. B. Goennenwein, and M. Weiler, *Applied Physics Letters* **110**, 092409 (2017).
- ⁵⁹ M. A. Nielsen and I. L. Chuang, *Quantum computation and quantum information* (Cambridge university press, 2010).
- ⁶⁰ G. Vidal and R. F. Werner, *Phys. Rev. A* **65**, 032314 (2002).
- ⁶¹ P. Liu, X.-M. Feng, and G.-R. Jin, *Chinese Physics B* **23**, 030310 (2014).
- ⁶² N. J. Cerf and C. Adami, *Phys. Rev. Lett.* **79**, 5194 (1997).
- ⁶³ M. Horodecki, J. Oppenheim, and A. Winter, *Nature* **436**, 673 (2005).
- ⁶⁴ T. Hioki, H. Shimizu, T. Makiuchi, and E. Saitoh, *Phys. Rev. B* **104**, L100419 (2021).
- ⁶⁵ R. Lescanne, L. Verney, Q. Ficheux, M. H. Devoret, B. Huard, M. Mirrahimi, and Z. Leghtas, *Phys. Rev. Applied* **11**, 014030 (2019).
- ⁶⁶ T. Srivastava, H. Merbouche, I. Ngouagnia Yemeli, N. Beaulieu, J. Ben Youssef, M. Muñoz, P. Che, P. Bortolotti, V. Cros, O. Klein, S. Sangiao, J. De Teresa, S. Demokritov, V. Demidov, A. Anane, C. Serpico, M. d'Aquino, and G. de Loubens, *Phys. Rev. Appl.* **19**, 064078 (2023).
- ⁶⁷ A. Asadian, C. Brukner, and P. Rabl, *Phys. Rev. Lett.* **112**, 190402 (2014).